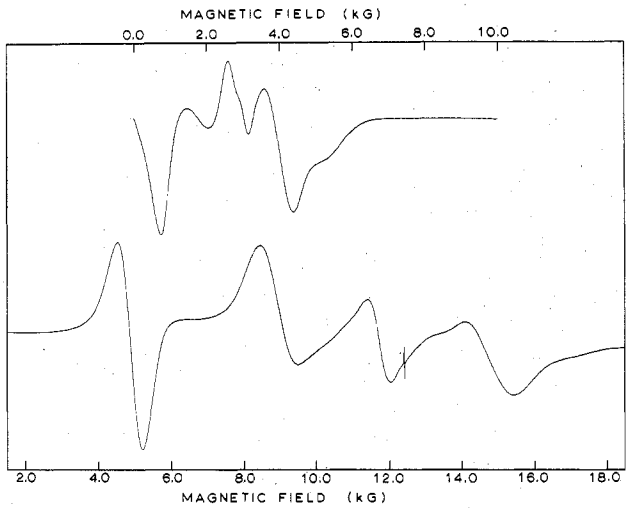

Figure 3. X-band (upper) and Q-band (lower) EPR spectra of powdered **1** at liquid-nitrogen temperature. The narrow resonance in the Q-band spectra is due to DPPH ($g = 2.0036$).

Cu–Cu separation of ≈3.6 Å fixes the maximum dipole–dipole zero-field splitting at 0.06 cm^{-1} or about 10% of the observed value. As has been presented in detail for another Cu(II) dimer, this difference in observed zero-field splitting and calculated maximum dipolar zero-field splitting is the result of an appreciable pseudo-dipolar zero-field interaction.[20] The ground electronic state of **1** is coupled with an excited state having a much larger value of J. The Q-band EPR spectrum (not shown) at ≈110 K for **2** is that of a magnetically dilute monomeric complex[21] having $g_\perp = 2.058$, $g_\parallel = 2.254$, and parallel copper hyperfine spacing of 191 G.

Acknowledgment. Research at Rutgers was supported by the National Institutes of Health (Grant AM-16412). Research at Illinois was supported by National Institutes of Health Grant HL-13652. We thank the authors of ref 6 for communicating the positional parameters of the title complex in advance of publication and also for the information presented as ref 21.

Registry No. $Cu_2(C_{12}H_{13}N_6O_2)_2H_2O{\cdot}2ClO_4$, 60583-90-6; $Cu(C_{12}H_{14}N_6O_2)_2{\cdot}2ClO_4$, 67421-38-9.

Supplementary Material Available: A table of experimental magnetic susceptibility data for **1** (1 page). Ordering information is given on any current masthead page.

References and Notes

(1) (a) Rutgers. (b) University of Illinois.
(2) E. I. Solomon, J. W. Hare, and H. B. Gray, *Proc. Natl. Acad. Sci. U.S.A.*, **73**, 1389 (1976).
(3) P. M. Coleman, H. C. Freeman, J. M. Guss, M. Murata, V. A. Norris, J. A. M. Ramshaw, and M. P. Venkatappa, *Nature (London)*, **272**, 319 (1978).
(4) D. Mastropaolo, J. A. Thich, J. A. Potenza, and H. J. Schugar, *J. Am. Chem. Soc.*, **99**, 424 (1977).
(5) (a) E. W. Wilson, Jr., M. H. Kasperian, and R. B. Martin, *J. Am. Chem. Soc.*, **92**, 5365 (1970). (b) G. F. Bryce and F. R. N. Gurd, *J. Biol. Chem.*, **241**, 1439 (1966).
(6) Figure 1 was constructed from atomic positional parameters reported by Y. Kojima, K. Hirotsu, and K. Matsumoto, *Bull. Chem. Soc. Jpn.*, **50**, 3222 (1977).
(7) (a) The unit cell of this complex contains a second crystallographically unique dimer which structurally is nearly identical with Figure 1. The corresponding dihedral angle of this other pseudotetrahedral CuN_4 site is 48.8°. (b) The copper–copper separation in the latter dimer is 3.600 (3) Å.
(8) C. C. Ou, D. A. Powers, J. A. Thich, T. R. Felthouse, D. N. Hendrickson, J. Potenza, and H. J. Schugar, *Inorg. Chem.*, **17**, 34 (1978).
(9) A. Earnshaw, "Introduction to Magnetochemistry", Academic Press, New York, N.Y., 1968.
(10) For example, the tetragonal[11] CuN_4O_2 chromophore present in $K_2(Cu(NH_2CHC(=O)NCH_2CO_2)_2){\cdot}6H_2O$ exhibits LF absorption at ≈535 nm.[12] Structurally analogous tetragonal $Cu(H_2NCH_2CH_2NH_2)_2X_2$ units where X is apically bound H_2O, Cl^-, Br^-, etc., exhibit LF absorption in the 520–535-nm range.[13]
(11) A. Sugihara, T. Ashida, Y. Sasada, and M. Kakudo, *Acta Crystallogr., Sect. B*, **24**, 203 (1968).
(12) Y. Nakao, K. Sakurai, and A. Nakahara, *Bull Chem. Soc. Jpn.*, **39**, 1608 (1966).
(13) V. M. Miskowski, J. A. Thich, R. Solomon, and H. J. Schugar, *J. Am. Chem. Soc.*, **98**, 8344 (1976).
(14) A. R. Amundsen, J. Whelan, and B. Bosnich, *J. Am. Chem. Soc.*, **99**, 6730 (1977).
(15) C. Bergman, E. Gandvik, P. O. Nyman, and L. Strid, *Biochim. Biophys. Res. Commun.*, **77**, 1052 (1977), and references cited therein.
(16) Copper(II)–disulfide bonding in low-molecular weight complexes is uncommon. Weak (apical) copper(II)–disulfide bonding has been reported by J. A. Thich, D. Mastropaolo, J. A. Potenza, and H. J. Schugar, *J. Am. Chem. Soc.*, **96**, 726 (1974).
(17) Supplementary material.
(18) For example, see G. F. Kokoszka and R. W. Duerst, *Coord. Chem. Rev.*, **5**, 209 (1970), and references therein. Similar Q-band EPR spectra have been observed in complexes with short Cu–Cu distances: C. J. Doumit, G. L. McPherson, R. L. Belford, S. B. Lenoux, and H. B. Jonassen, *Inorg. Chem.* **16**, 565 (1977).
(19) E. Wasserman, L. C. Snyder, and W. A. Yager, *J. Chem. Phys.*, **41**, 1763 (1964).
(20) T. T. Felthouse and D. N. Hendrickson, *Inorg. Chem.*, **17**, 444 (1978).
(21) A dihydrate form of **2**, $Cu(C_{12}H_{14}N_6O_2)_2{\cdot}2ClO_4{\cdot}2H_2O$, contains discrete $Cu(C_{12}H_{14}N_6O_2)_2^{2+}$ cations; puckered CuN_4 units arise from the ligation of Cu(II) by the four imidazole residues. Private communication from Dr. Keiji Matsumoto, Osaka City University, Osaka, Japan.

Contribution from the Department of Chemistry, University of British Columbia, Vancouver, British Columbia, Canada V6T 1W5

$X\alpha$ Scattered-Wave Calculations of the Electronic Structures of SO_2 and SO_2F_2. Relationship to π Bonding in the Cyclic Phosphazenes

L. NOODLEMAN and K. A. R. MITCHELL*

Received December 14, 1977

The overlapping-spheres $X\alpha$ scattered-wave method has been used for investigating the chemical bonding and the electronic structures of SO_2 and SO_2F_2. Excellent agreement is obtained for SO_2 both with the experimental photoelectron spectrum and with the charge distributions obtained previously with near-Hartree–Fock calculations. For SO_2F_2, there is also good agreement with the observed He I and He II spectra, and molecular orbital contour maps have been used for discussing the vibrational structure in the He I spectrum. These new calculations demonstrate a close connection between the level ordering and π bonding in SO_2F_2 and the corresponding quantities obtained in earlier $X\alpha$ scattered-wave calculations on the cyclic phosphazene fluorides $(NPF_2)_3$ and $(NPF_2)_4$.

Introduction

There is a continuing interest in the nature of the chemical bonding in molecules of phosphorus or sulfur in which the second-row atom is in a high formal oxidation state, and previous discussions have tended to center on the role of 3d orbitals.[1,2] More recently a number of important computational methods have become sufficiently developed to allow the quantitative investigation of the electronic structures of

Table I. Sphere Radii[a] and α Parameters

	radius		α parameter	
	SO_2	SO_2F_2[b]	SO_2	SO_2F_2
S	1.729	1.652, 1.790	0.72475	0.72475
O	1.515	1.535, 1.663	0.74447	0.74447
F		1.550, 1.679		0.73732
outer sphere	4.391	4.442, 4.571	0.73773	0.73767
intersphere			0.73773	0.73767

[a] In units of the Bohr radius (a_0). [b] Sphere radii for 20 and 30% overlap models, respectively, for SO_2F_2.

such molecules and comparison with experimental data.[3,4]

In the present paper we focus on SO_2, SO_2F_2, and the cyclic phosphazenes. These are molecules for which 3d orbitals have been proposed as being important in π bonding,[5] although this model has not been universally accepted. For example, SO_2 has been a favorite textbook case and it has often been treated as an analogue of O_3,[6] such that the bonding is considered to involve resonance between ionic forms like

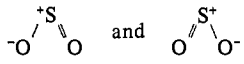

which maintain the octet at sulfur, even though the trends in bond lengths are not immediately consistent with this (e.g. the O–O distance in O_3 is 0.07 Å longer than in O_2, but the S–O distance in SO_2 is 0.06 Å shorter than in SO).[7] An alternative first approximation corresponds to the structure

based on localized electron pair bonds and involving one d electron at sulfur.

The cyclic phosphazenes provide another important type of system with significant implications for chemical bonding models,[8] and we have recently made some Xα scattered-wave (Xα SW) calculations[9] to help interpret the photoelectron spectra of $(NPF_2)_3$ and $(NPF_2)_4$. The aim of the present paper is to investigate the electronic structures of SO_2 and SO_2F_2, which both contain a common V-shaped SO_2 moiety, and to compare the orbital level structure and π bonding in SO_2F_2 with those found in the previous calculations for $(NPF_2)_3$ and $(NPF_2)_4$. The latter comparison depends on the similar structural arrangements around sulfur and phosphorus, respectively. SO_2 and SO_2F_2 are less complex molecules than the phosphazenes and more detailed experimental data are available for the former systems, for example, vibrational fine structure in the He I photoelectron spectra.[10,11] This enables theoretical studies of SO_2 and SO_2F_2 to be tested more completely than is possible at present for the phosphazenes.

Specification of Calculations

The calculations on SO_2 and SO_2F_2 employed the same 20% overlapping-spheres version of the Xα SW method that we used for other loosely packed molecules like $(NPF_2)_{3,4}$ and P_4S_3.[9,12] The use of a fixed overlap provides a common basis for comparing atomic orbital populations and charge distributions in SO_2, SO_2F_2, and $(NPF_2)_{3,4}$. Table I summarizes the parameters used in the calculations. The ratios of sphere sizes were obtained by the procedure described by Norman,[13] and we used the exchange correlation parameters determined by Schwarz.[14] To determine the dependence of the calculated electronic structure on sphere overlap, ground-state calculations for SO_2F_2 were also made with 30% overlap.

Ionization energies were calculated using Slater's Xα transition-state method[15,16] for both SO_2 and SO_2F_2. The calculations employed partial wave expansions to $l = 1$ for the oxygen and fluorine spheres; the basis was extended to $l = 2$ functions for the sulfur spheres and to $l = 4$ for the outer spheres. All calculations have been made with the bond lengths and bond angles found experimentally,[17,18] and the coordinate systems used are indicated in Figure 1. Table II gives the irreducible

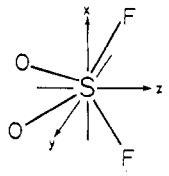

Figure 1. Specification of the axes used for SO_2F_2 and SO_2. The x axis is perpendicular to the OSO plane and the z axis is the twofold rotation axis. The F atoms are in the xz plane. Similar local axes are used at P in $(NPF_2)_{3,4}$ with the x axis perpendicular to the PN ring.

Table II. Some Useful Symmetry Classifications for the C_{2v} Point Group

representation	E	C_2	σ_v (xz)	σ_v' (yz)	d orbitals	classification[a]
a_1	1	1	1	1	z^2, x^2-y^2	homomorphic, in-plane
a_2	1	1	−1	−1	xy	heteromorphic, out-of-plane
b_1	1	−1	1	−1	xz	homomorphic, out-of-plane
b_2	1	−1	−1	1	yz	heteromorphic, in-plane

[a] Used later in discussion on cyclic phosphazenes.

Table III. Calculated and Experimental Ionization Energies (in eV) for SO_2

level	Xα SW 20% overlap[a]	Xα SW 33% overlap[b]	near-Hartree–Fock[c]	experiment[d]
$4a_1$	12.51	12.03	13.38	12.45
$3b_2$	13.00			
$1a_2$	13.40	13.20 (av)	12.84 (av)	14.37 (av)	13.30 (av)
$1b_1$	15.26			
$3a_1$	15.70	16.60 (av)	16.14 (av)	18.69 (av)	16.60 (av)
$2b_2$	18.53			
$2a_1$	21.71	20.34	23.66	20.65

[a] This work, calculations use transition-state theory. [b] Reference 13; nearly perfect agreement with the virial theorem is obtained with this degree of overlap. [c] Reference 19, with use of Koopmans' theorem. [d] From ref 13; represents an average of four independent determinations by photoelectron spectroscopy.

representations of the C_{2v} point group for both SO_2 and SO_2F_2 with $\sigma_v(xz)$ specifying the mirror plane which bisects the OSO angle and $\sigma'_v(yz)$ the mirror plane which coincides with the OSO plane.

Ionization Energies and Bonding in SO_2

Ionization energies calculated in this work with 20% overlap in the Xα SW transition-state procedure are given in Table III; comparison is made with values from experiment, from similar calculations with 33% overlap,[13] and from calculations using the near-Hartree–Fock method in conjunction with Koopmans' theorem.[19] The same level ordering is found for the two sets of Xα SW calculations; the shift from 33 to 20% overlap increases the calculated ionization energies by 0.5–1.4 eV, with the larger increases corresponding to the lower levels. There is a single discrepancy between the Xα SW and the near-Hartree–Fock level orderings in Table III; the latter calculations interchange the ordering of the $1a_2$ and $3b_2$ levels compared with the Xα SW calculations. Very recently Cederbaum and his co-workers[20] have discussed the "difficult assignment" of the lowest ionic states of O_3 and SO_2 using many-body perturbation theory. They have used extensive basis sets, calculated the vibrational fine structures, and concluded, for the two closely spaced levels (separation 0.3 eV) in the second band of the photoelectron spectrum of SO_2,[21] that $1a_2$ is probably at lower binding energy than $3b_2$. This

Table IV. One-Electron Energy Eigenvalues and Partial-Wave Decompositions[a] for SO_2

level	energy eigenvalue[b]	S			2 O		outer sphere[c]	inter-sphere[c]
		3s	3p	3d	2s	2p		
$1a_1$	−2.177	0.277	0.034	0.018	0.508	0.073	0.008	0.081
$2a_1$	−1.292	0.287	0.002	0.000	0.288	0.235	0.038	0.150
$3a_1$	−0.866	0.037	0.267	0.006	0.004	0.404	0.087	0.195
$4a_1$	−0.626	0.071	0.098	0.066	0.002	0.521	0.066	0.175
$1a_2$	−0.682	0	0	0.031	0	0.729	0.024	0.216
$1b_1$	−0.835	0	0.227	0.005	0	0.455	0.030	0.283
$1b_2$	−2.006	0	0.149	0.033	0.698	0.049	0.009	0.062
$2b_2$	−1.050	0	0.177	0.014	0.103	0.570	0.025	0.111
$3b_2$	−0.651	0	0.004	0.026	0.000	0.745	0.053	0.172

atomic-sphere populations: S $(3s)^{1.34}$ $(3p)^{1.91}$ $(3d)^{0.40}$; O $(2s)^{1.60}$ $(2p)^{3.78}$

net atomic charges:[d] $S^{+1.15}$ $O^{-0.57}$

[a] From Xα SW calculations with 20% overlap; all partial waves are normalized to unity for each molecular orbital. [b] In rydbergs. [c] Total charge in region. [d] Atomic-sphere radii have been chosen in the ratio of the neutral-atom radii obtained after superimposing atomic charge densities as in ref 13. The total outer-sphere and intersphere charge has been allocated equally to each atom.

ordering is consistent with the near-Hartree–Fock calculations and differs from that given by the Xα SW calculations.

Table IV gives the ground-state eigenvalues for the whole of the valence region, from the 20% overlap calculations, as well as a detailed partial-wave analysis of the molecular orbitals. Contour maps from the 20% Xα SW calculations for some selected molecular orbitals are shown in Figure 2. The highest occupied molecular orbital ($4a_1$) displays weak bonding between an essentially pure 2p orbital at oxygen and an orbital at sulfur with mixed spd character (Figure 2a). The $3b_2$ and $1a_2$ orbitals are oxygen $2p_\pi$ states with some weak π bonding to sulfur. The d-type symmetry on sulfur for $3b_2$ is clearly evident in Figure 2b, and similar d participation is present in $1a_2$. The $1b_1$ and $3a_1$ orbitals are O(2p)–S(3p) π bonds out of the molecular plane and in the molecular plane, respectively, and $3a_1$ is plotted in Figure 2c. The $2b_2$ and $1b_2$ states represent S(3p)–O(2p) and S(3p)–O(2s) σ bonds, respectively (Figure 2d,e). The $2a_1$ orbital involves essentially nonbonding interactions between S(3s) and O(2s/2p) (Figure 2f), while $1a_1$ corresponds to S(3s)–O(2s) bonding.

To provide an independent check on these Xα SW calculations, we compare the overall electron distributions with those from the near-Hartree–Fock calculations.[19] A Mulliken population analysis yields $S^{+1.13}O^{-0.565}{}_2$ for the Hartree–Fock calculations, whereas the 20% Xα SW calculation gives $S^{+1.15}O^{-0.575}{}_2$ (Table IV). The total d function populations are 0.40 and 0.43 for the 20% Xα SW calculation and for the near-Hartree–Fock calculation, respectively. However, since for the former the d population is dependent on sphere size, it seems more satisfactory to compare the percentage d character on sulfur. These are 11.0 and 8.7% for the Xα SW and Hartree–Fock calculations, respectively. The effects of including d functions at sulfur in the basis sets seem broadly comparable in these two sets of calculations. For example, the lowering in total energy is 205 kcal mol^{-1} for the Xα SW calculation and 162 kcal mol^{-1} for the near-Hartree–Fock calculation.

This evidence suggests that the basic bonding and charge-distribution characteristics are similar from the near-Hartree–Fock and Xα SW calculations.[22] For molecules larger than SO_2 calculations at the near-Hartree–Fock level become progressively more time-consuming; indeed, anticipating our discussion of SO_2F_2, we note here that no near-Hartree–Fock calculation has yet been made for this latter molecule. However, a minimum basis set linear combination of atomic orbital (LCAO) calculation has been made, and that makes it relevant to mention briefly a similar LCAO calculation for SO_2.[23] This calculation indicated a very high d population on sulfur (1.17 electron), a total energy of −541.008 hartrees (compare −547.209 and −546.278 hartrees for the near-Hartree–Fock and 20% Xα SW calculations, respectively) and a first ionization energy which is 1.3 eV less than the value from the near-Hartree–Fock calculation.[24]

Table V. Ionization Energies (in eV) and Vibrational Spacings (in cm^{-1}) for SO_2F_2

level[a]	LCAO[b]	Xα SW[c]	exptl[d]	vib spacing[e]	vib assignt[f]
$4b_2$	13.7	15.18	13.55	370	ν_3 or ν_4
$2a_2$	14.3	15.48	13.81	475	ν_3
$4b_1$	15.8	16.07	15.18	340	ν_4
$6a_1$	16.2	16.51	15.31	1025	ν_1
$3b_2$	17.3	18.80	16.68	1135, 805, 510	ν_1, ν_2, ν_3
$3b_1$	19.1	18.96			
$1a_2$	20.5	19.43	18.31		
$5a_1$	19.7	19.60			
$2b_2$	21.9	20.66	19.39	850, 485	ν_2, ν_3
$4a_1$	21.9	21.14	19.81	855, 500	ν_2, ν_3
$2b_1$	23.4	22.13	21.7		
$3a_1$	26.0	25.12[g]	24.2		

[a] Designations for valence shell. [b] Minimum basis set calculation with Koopmans' theorem; ref 10. [c] From transition-state calculations with Xα SW model for 20% overlap; this work. [d] Vertical ionization energies from ref 10 except those for $4b_2$ and $2a_2$ are from ref 11. [e] From ref 10. [f] Ground-state molecular vibrations of A_1 symmetry from ref 25 are ν_1(SO str) = 1269 cm^{-1}, ν_2(SF stretch) = 848 cm^{-1}, ν_3(OSO bend) = 544 cm^{-1}, ν_4(FSF bend) = 384 cm^{-1}. [g] Value estimated by adding the $2b_1$ relaxation energy (i.e., difference between one-electron eigenvalue and the corresponding transition-state energy) to the $3a_1$ one-electron eigenvalue.

Photoelectron Spectra Assignments and Bonding in SO_2F_2

Transition-state ionization energies calculated with the 20% overlapping-spheres Xα SW method for SO_2F_2 are reported in Table V and compared both with experimental values[10,11] and with values previously reported from an LCAO calculation which used a minimum basis set including 3d orbitals at sulfur.[10] The He I and He II photoelectron spectra for SO_2F_2 are shown in Figure 3, and included as well are our calculated values which have been reduced by 1.35 eV, from the values in Table V, in order to improve the correspondence between calculation and experiment. The vibrational progressions observed for some bands are given in Table V. These are useful for comparing with the nature of the calculated molecular orbitals (contour maps are given in Figure 4) and for thereby assessing our assignments of the photoelectron spectra. Table VI gives atomic charges and a partial-wave analysis of the molecular orbitals from our Xα SW calculations on SO_2F_2.

We assign the highest energy band found by He I to ionization from the $4b_2$ and $2a_2$ levels; the corresponding contour maps are given in Figure 4a,b. These states correspond

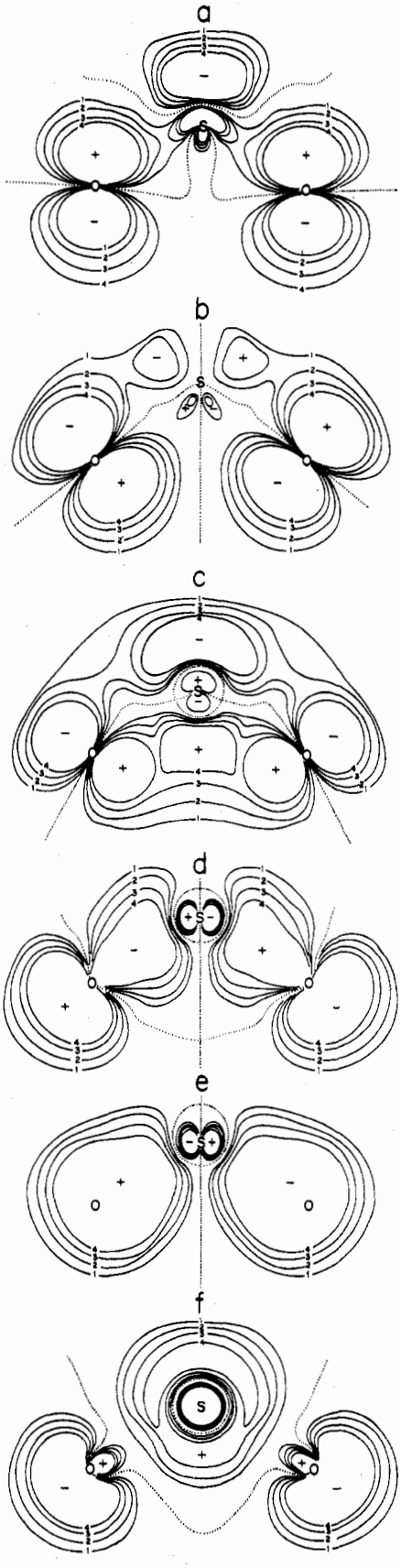

Figure 2. Wave function contour diagrams for SO_2: (a) $4a_1$, (b) $3b_2$, (c) $3a_1$, (d) $2b_2$, (e) $1b_2$, (f) $2a_1$. The contour specifications are 1 = 0.05, 2 = 0.07, 3 = 0.10, and 4 = 0.13 in units of (probability)$^{1/2}$ a_0^{-3}; each dotted line represents the intersection with a nodal surface. For reasons of clarity, some inner contours have not been drawn.

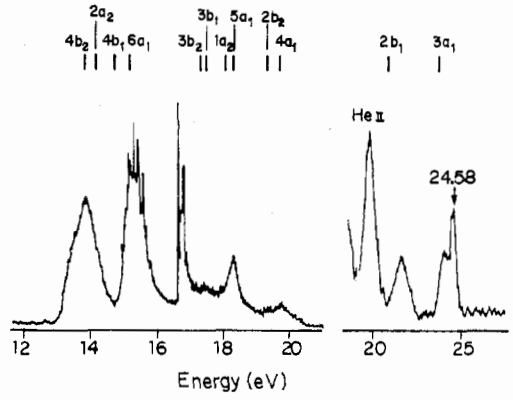

Figure 3. Comparison for SO_2F_2 of ionization energies calculated with the 20% overlapping-sphere Xα SW method and the He I and He II photoelectron spectra from ref 10. The calculated ionization energies have been shifted uniformly by 1.35 eV to lower energies.

to weakly bonding O $2p_\pi$ molecular orbitals and are consistent with excitation of the ν_3 (OSO bending) mode. The second band is assigned to ionization from $4b_1$ and $6a_1$. The $4b_1$ orbital manifests both S–O π bonding and S–F antibonding interactions (Figure 4c,d), while the $6a_1$ orbital corresponds to O–S–O π bonding (Figure 4e). The S–F and F–F antibonding interactions in $4b_1$ are consistent with excitation of the ν_4 (FSF bending) mode, and the S–O π bonding in $6a_1$ is also in accordance with the excitation of ν_1 (SO stretch). Excitation of ν_1 may also be expected with ionization from $4b_1$, but it has not been observed. In the third band, the principal progression involves ν_1 (SO stretch) with subsidiary progressions for ν_2 (SF stretch) and ν_3 (OSO bending). The $3b_2$ orbital assigned to this band contains both S–O bonding and S–F nonbonding contributions (Figure 4f,g). While more charge resides on F than on O in $3b_2$, the vibrational structure is expected to be more sensitive to the bonding than to the nonbonding contributions; the S–O principal progression is not therefore surprising. The location of the $3b_1$ F–F nonbonding state (Figure 4h) is uncertain; it may lie under the $3b_2$ band envelope (peaked at 16.68 eV in the He I spectrum) or it may lie between 17 and 18 eV where the spectrum (Figure 3) shows an unusually high background. The fourth band is fairly wide and has no resolved fine structure; this seems consistent with our assignment to two F 2p lone pair states, $1a_2$ and $5a_1$. The fifth band has two observable components; both display ν_2 (SF) and ν_3 (OSO) progressions and the $2b_2$ and $4a_1$ states assigned to this band show both S–O and S–F bonding (Table VI; Figure 4i,j). The next two bands, obtained with He II radiation, are attributed respectively to the $2b_1$ S–F σ state (Figure 4k) and to the $3a_1$ state, which involves S–F σ bonding and an sp nonbonding combination at oxygen (Figure 4l). The states $1a_1$, $1b_1$, $2a_1$, and $1b_2$, not seen with He I or He II photoelectron spectroscopy, mainly involve the fluorine 2s and oxygen 2s atomic orbitals and some interaction with sulfur.

The bonding characteristics found for the molecular orbitals from the Xα SW calculations are broadly consistent with the vibrational structure observed in the photoelectron spectra, although it is clear that a vibrational analysis alone is not sufficient for unambiguously determining the level assignments. It is also significant that the Xα SW calculations reproduce quite well the spacings between bands as well as the spacings between components within a band. In addition to the calculations with the 20% overlapping-spheres model, we have also calculated the ground-state electronic structure of SO_2F_2 with 30% overlap. A comparison of the two sets of the ground-state one-electron eigenvalues is given in Table VII, and on the average the 30% overlap model gives orbital energies which are 1.4 eV higher. This strongly suggests that

Table VI. Partial-Wave Decompositions[a] for SO_2F_2

	S			2 O		2 F			
level	3s	3p	3d	2s	2p	2s	2p	outer sphere	inter-sphere
$1a_1$	0.124	0.008	0.000	0.035	0.009	0.689	0.012	0.007	0.115
$2a_1$	0.171	0.047	0.021	0.476	0.061	0.127	0.004	0.005	0.087
$3a_1$	0.185	0.037	0.004	0.185	0.066	0.053	0.317	0.028	0.126
$4a_1$	0.024	0.137	0.005	0.090	0.294	0.004	0.260	0.028	0.147
$5a_1$	0.002	0.010	0.019	0.004	0.061	0.000	0.716	0.019	0.167
$6a_1$	0.000	0.009	0.051	0.000	0.613	0.000	0.052	0.024	0.249
$1a_2$	0	0	0.012	0	0.029	0	0.770	0.015	0.173
$2a_2$	0	0	0.023	0	0.682	0	0.055	0.020	0.220
$1b_1$	0	0.026	0.010	0	0.000	0.864	0.003	0.010	0.086
$2b_1$	0	0.171	0.010	0	0.037	0.018	0.599	0.026	0.139
$3b_1$	0	0.000	0.010	0	0.001	0.000	0.820	0.018	0.138
$4b_1$	0	0.025	0.028	0	0.538	0.002	0.152	0.023	0.231
$1b_2$	0	0.146	0.024	0.692	0.046	0	0.002	0.006	0.084
$2b_2$	0	0.139	0.000	0.092	0.358	0	0.228	0.028	0.154
$3b_2$	0	0.034	0.030	0.012	0.252	0	0.514	0.027	0.131
$4b_2$	0	0.002	0.016	0.000	0.702	0	0.048	0.020	0.211

atomic-sphere populations: $S\ (3s)^{1.01}\ (3p)^{1.58}\ (3d)^{0.53}$; $O\ (2s)^{1.59}\ (2p)^{3.76}$; $F(2s)^{1.76}\ (2p)^{4.56}$

net atomic charges:[b] $S^{+1.96}\ O^{-0.43}\ F^{-0.55}$

[a] From Xα SW calculations with 20% overlap. [b] Obtained by allocating the outer-sphere charge equally to the O and F atoms; the inter-sphere charge is allocated to atoms in the ratios of the number of valence electrons.

Table VII. One-Electron Xα SW Eigenvalues[a] for SO_2F_2

level	20% overlap	30% overlap	level	20% overlap	30% overlap
$1a_1$	−2.613	−2.525	$1b_1$	−2.511	−2.415
$2a_1$	−2.282	−2.214	$2b_1$	−1.318	−1.241
$3a_1$	−1.538	−1.428	$3b_1$	−1.062	−0.954
$4a_1$	−1.265	−1.162	$4b_1$	−0.895	−0.768
$5a_1$	−1.132	−1.029	$1b_2$	−2.143	−2.083
$6a_1$	−0.922	−0.802	$2b_2$	−1.227	−1.123
$1a_2$	−1.106	−0.998	$3b_2$	−1.093	−0.994
$2a_2$	−0.841	−0.706	$4b_2$	−0.816	−0.677

[a] In rydbergs.

transition-state energies obtained with the 30% overlapping-spheres model would give good absolute agreement with the ionization energies measured for SO_2F_2. The level ordering is the same from both models, and both yield very similar partial-wave analyses and charge distributions for all the molecular orbitals. We find the virial ratio $-2T/V$ to be 1.0034 and 1.0007 for the 20% and the 30% overlap models, respectively, and these observations give support to the suggestion of Norman[13] that consistency with the virial theorem be used as the criterion for choosing absolute sphere radii. Although agreement with the virial theorem does not always yield optimum ionization energies,[12] it does appear to provide a uniform procedure for predicting ionization energies to within 1 eV or so for a wide variety of molecular systems.

The assignment of the photoelectron spectra of SO_2F_2 by DeKock et al.[10] was based on their minimum basis set LCAO calculation. Their level ordering agrees with ours except for a switching of the $1a_2$ and $5a_1$ levels, which are separated by 0.17 eV in the Xα SW calculation and by 0.8 eV in the LCAO calculation (Table V). However, there are differences in the assignments of the bands in the photoelectron spectra because the level spacings are different from the two types of calculations. The level spacings from the LCAO calculation provide a poorer match to the experimental spectra, with regard to both separations between bands and between components within a band, than those from the Xα SW calculation, and this is particularly so for the lower valence levels. For example, on the basis of the LCAO calculation, ionizations from $1a_2$ (20.5 eV) and $2b_2$ (21.9 eV) are assigned to a single-measured vertical ionization energy at 19.39 eV. Nevertheless, the absolute deviation of the LCAO ionization energies from experiment is 1.13 eV, and this is somewhat better than the average deviation of 1.35 eV with the 20% Xα SW model. DeKock et al. report Mulliken population analyses for all of their valence molecular orbitals,[10] and this permits comparisons with our charge distributions in Table VI. We find substantial discrepancies between the two methods in four of the sixteen molecular orbitals, namely, $3b_2$, $5a_1$, $2b_2$, and $4a_1$. However, there are no significant discrepancies in charge distributions or level assignments for the first two bands which correspond to ionization of the S–O π bonds.

Relationships in the Level Structure of SO_2, SO_2F_2, and $(NPF_2)_{3,4}$

To help the development of improved models for the bonding and electronic structures of the types of molecules of interest in this paper, it is important that the basic relationships in the level structures are established on the basis of reliable calculations (e.g., those that compare well with measured ionization energies). Figure 5 compares the ionization energies that have been calculated for SO_2 and SO_2F_2 with the 20% overlapping-spheres Xα SW method, but for SO_2F_2 the energies have been shifted, as previously, by 1.35 eV. An appreciable consistency is evident in the changes in levels on forming SO_2F_2 from SO_2 and two F atoms. For example, below the highest occupied $4a_1$ orbital for SO_2, the level ordering b_2, a_2, b_1, a_1 is preserved in the two molecules. From analysis of energies and orbital characteristics (Tables IV and VI; Figures 2 and 4), the following correlations (as marked on Figure 5) are established for sets of states for SO_2 and SO_2F_2, respectively: ($3b_2$, $4b_2$), ($1a_2$, $2a_2$), ($1b_1$, $2b_1$ and $4b_1$), ($3a_1$ and $4a_1$, $4a_1$ and $6a_1$), ($2b_2$, $2b_2$ and $3b_2$), ($2a_1$, $3a_1$), ($1a_1$, $2a_1$), ($1b_2$, $1b_2$).

The orbitals in the five sets ($3b_2$, $4b_2$), ($1a_2$, $2a_2$), ($2a_1$, $3a_1$), ($1a_1$, $2a_1$), and ($1b_2$, $1b_2$) are basically similar in SO_2 and SO_2F_2, respectively, and we now concentrate on the relationships that involve important modifications. For the high-lying a_1 levels, about half an electron is transferred from sulfur, in the orbitals $3a_1$ and $4a_1$ of SO_2, into the fluorine atoms in orbital $4a_1$ of SO_2F_2, and this continues to S–F bonding. This same interaction yields the $6a_1$ orbital of SO_2F_2 for which the OSO π system involves mainly d character on sulfur; this involvement contrasts with those in the $3a_1$ and $4a_1$ states of SO_2. The $1b_1$ orbital in SO_2 is changed in the interaction with two fluorine atoms to give more S–F σ bonding, in the orbital $2b_1$ of SO_2F_2, and the high-lying orbital $4b_1$ which corresponds to S–O out-of-plane π bonding with

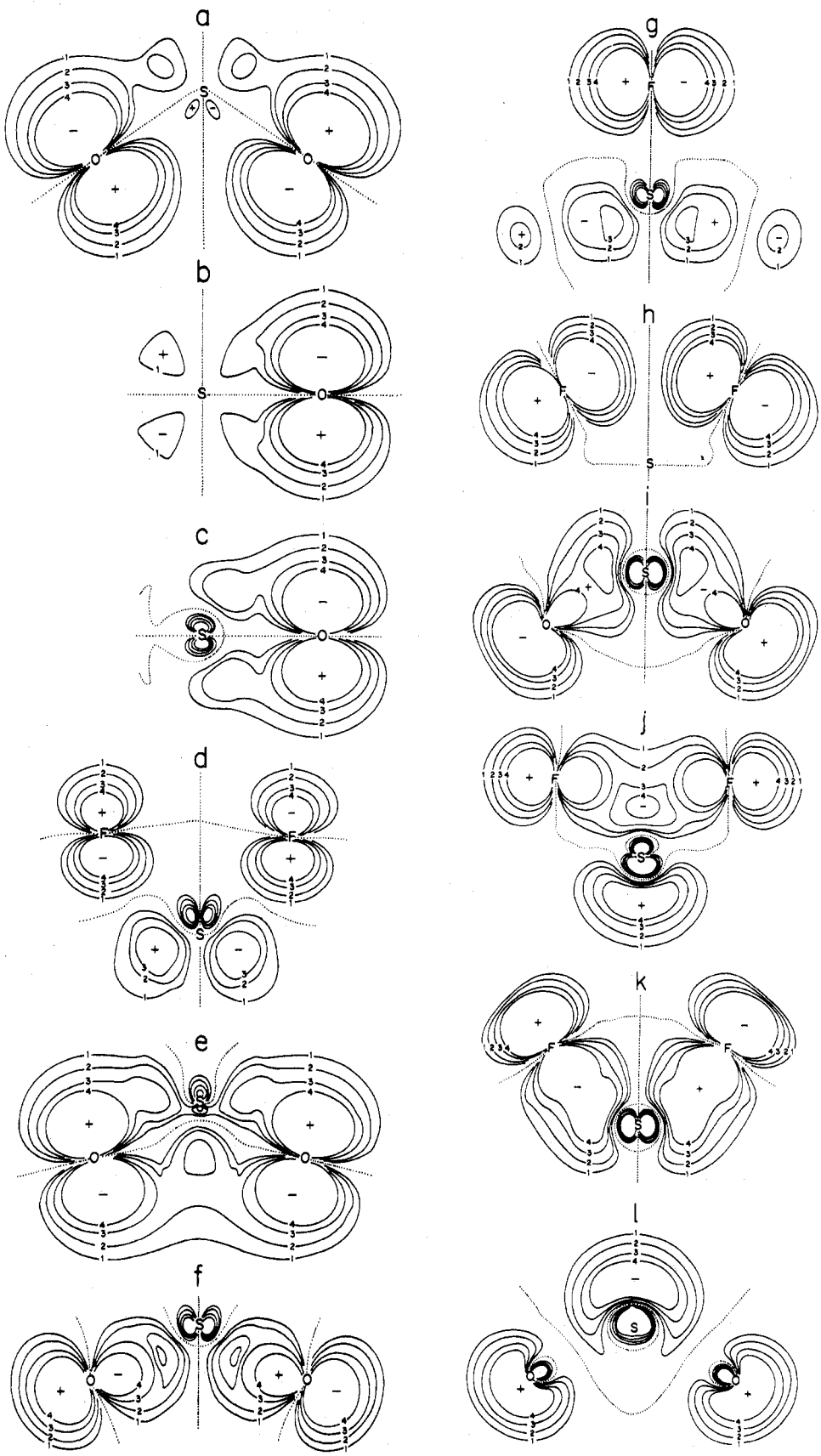

Figure 4. Wave function contour diagrams for SO_2F_2: (a) $4b_2$ in yz plane, (b) $2a_2$ in plane perpendicular to yz plane, (c) $4b_1$ in plane perpendicular to yz plane, (d) $4b_1$ in xz plane, (e) $6a_1$ in yz plane, (f) $3b_2$ in yz plane, (g) $3b_2$ in a plane at 48° to yz plane, (h) $3b_1$ in xz plane, (i) $2b_2$ in yz plane, (j) $4a_1$ in xz plane, (k) $2b_1$ in xz plane, (l) $3a_1$ in yz plane. The contour specifications are given in Figure 2.

nearly equal S(3p) and S(3d) contributions. The $2b_2$ orbital in SO_2 corresponds to an S–O σ bond, and this is preserved in SO_2F_2, although the interaction with $F(2p_\pi)$ orbitals provides in addition S–F antibonding and S–F π-bonding components in $3b_2$ and $2b_2$, respectively. The levels $3b_1$, $1a_2$, and $5a_1$ correspond to nonbonding $F(2p_\pi)$ orbitals, and, along

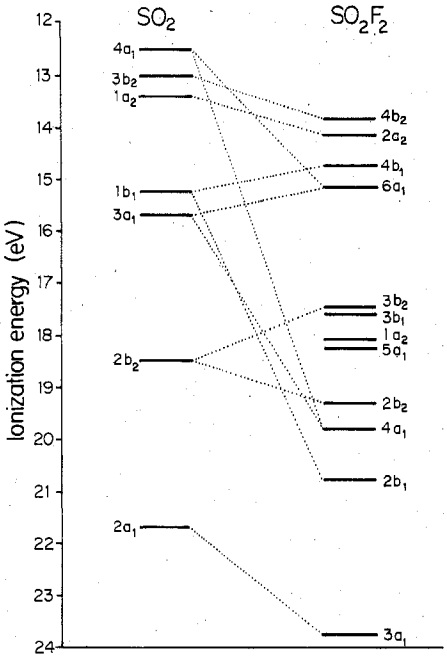

Figure 5. Comparison of the ionization energies calculated with the 20% overlapping-sphere Xα SW method for SO_2 and SO_2F_2; the values for SO_2F_2 have been shifted uniformly by 1.35 eV to lower energies.

with the F component of $3b_2$, they essentially compose the F(2p) nonbonding band in SO_2F_2.

Comparisons are now made between SO_2F_2 and $(NPF_2)_{3,4}$ with emphasis on the π characters of the SO and PN bonds. This comparison is suggested since, in the phosphazene fluorides, phosphorus is surrounded by two nitrogens and two fluorines in close analogy with sulfur being surrounded by two oxygens and two fluorines in SO_2F_2. The C_{2v} group for SO_2F_2 corresponds to the site symmetry at phosphorus in the phosphazenes; moreover, the bond angles match closely: N–P–N = 120°, F–P–F = 100° in $(NPF_2)_3$,[26] and O–S–O = 124°, F–S–F = 96° in SO_2F_2.[18] The terminology that has frequently been used in classifying phosphazene molecular orbitals is specified in Table II along with the representations of the d functions at P (or at S in SO_2 or SO_2F_2). The terms "in-plane" and "out-of-plane" refer to functions symmetric or antisymmetric, respectively, to the NPN or OSO planes, while homomorphic and heteromorphic specify functions symmetric or antisymmetric, respectively, to planes which are perpendicular to the NPN or OSO angles and bisect them.

The total number of π electrons in the in-plane and out-of-plane systems in $(NPF_2)_3$ and $(NPF_2)_4$ are 12 and 16, respectively, or four π electrons per monomer unit. There are eight electrons in the analogous π systems of SO_2F_2, and so it is to be expected that two of the four π orbitals which are occupied in SO_2F_2 will be unoccupied in the phosphazene fluorides. Consistent with this the two highest levels in SO_2F_2, namely, $4b_2$ and $2a_2$, are not represented in the occupied level structures of $(NPF_2)_{3,4}$ according to the previous analysis with Xα SW calculations.[9] The next highest orbital in SO_2F_2, namely, the $4b_1$ level, corresponds to the two highest levels (7e″, $6a_2$″) in $(NPF_2)_3$ and to three of the four highest levels ($2b_{1u}$, $7e_g$, $6a_{2u}$) in $(NPF_2)_4$. These are all homomorphic out-of-plane π systems. Likewise the $6a_1$ level in SO_2F_2 corresponds to the (13e′, $10a_1$′) levels in $(NPF_2)_3$ and to the ($5b_{2g}$, $13e_u$, $10a_{1g}$) levels in $(NPF_2)_4$; these are all homomorphic in-plane π systems.

Partial-wave analyses and calculated ionization energies for the PN π orbitals[9] in $(NPF_2)_{3,4}$ are presented in Table VIII. Contour maps of the in-plane π orbitals are given in Figure 6; these are the most strongly bonding of the ring π orbitals.

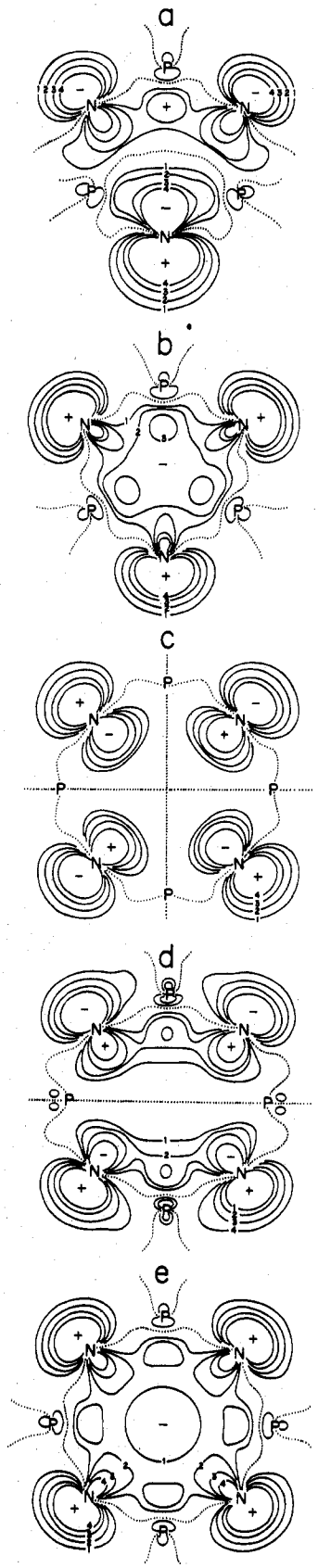

Figure 6. Wave function contour diagrams for (a) 13e′ and (b) $10a_1$′ of $(NPF_2)_3$ and (c) $5b_{2g}$, (d) $13e_u$, and (e) $10a_{1g}$ of $(NPF_2)_4$. The contour specifications are given in Figure 2.

A comparison of these plots and the corresponding partial-wave analyses, with those for $6a_1$ in SO_2F_2, shows a general similarity in the bonding characteristics, although the phos-

Table VIII. Ionization Energies[a] and Partial-Wave Decompositions for Ring π Systems in $(NPF_2)_{3,4}$[b]

set[c]	level	ionization energy	ΣP 3s	ΣP 3p	ΣP 3d	ΣN 2s	ΣN 2p	ΣF 2s	ΣF 2p	vacancy sphere	outer sphere	inter-sphere
I	$7e''$	10.81	0	0.014	0.037	0	0.629	0.001	0.059	0.006	0.001	0.252
	$6a_2''$	11.81	0	0.040	0.044	0	0.496	0.003	0.113	0.023	0.003	0.278
II	$13e'$	12.94	0.005	0.049	0.047	0.055	0.616	0.000	0.006	0.054	0.003	0.164
	$10a_1'$	15.84	0.021	0.052	0.042	0.192	0.356	0.000	0.047	0.130	0.002	0.158
III	$2b_{1u}$	9.79	0	0.000	0.040	0	0.654	0.000	0.047	0.021	0.000	0.238
	$7e_g$	10.41	0	0.027	0.040	0	0.568	0.002	0.074	0.032	0.002	0.253
	$6a_{2u}$	11.10	0	0.039	0.040	0	0.477	0.003	0.102	0.056	0.002	0.281
IV	$5b_{2g}$	10.66	0.000	0.001	0.033	0.013	0.674	0.000	0.038	0.119	0.002	0.121
	$13e_u$	12.08	0.003	0.034	0.057	0.044	0.574	0.000	0.018	0.135	0.002	0.133
	$10a_{1g}$	13.93	0.012	0.041	0.050	0.117	0.447	0.000	0.010	0.190	0.001	0.133

[a] Values in eV calculated with the transition-state theory. [b] Calculations specified in ref 9. [c] I and II are for $(NPF_2)_3$, III and IV for $(NPF_2)_4$, I and III are for the out-of-plane homomorphic π system, and II and IV are for the in-plane homomorphic π system.

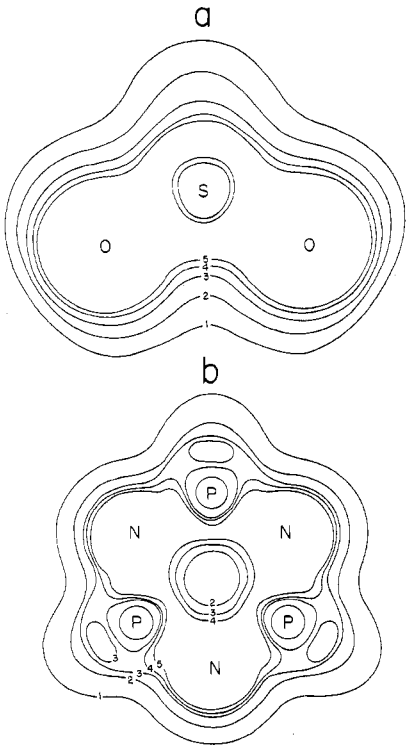

Figure 7. Valence electron charge distributions in yz planes for (a) SO_2F_2 with contour specifications 1 = 0.006, 2 = 0.015, 3 = 0.034, 4 = 0.056, and 5 = 0.080 electrons a_0^{-3} and (b) $(NPF_2)_3$ with 1 = 0.006, 2 = 0.023, 3 = 0.055, 4 = 0.084, and 5 = 0.122 electrons a_0^{-3}.

phazenes display greater degrees of 3p–3d mixing at the second-row atoms. Similar close resemblances are found between the weakly bonding out-of-plane π systems in $(NPF_2)_{3,4}$ and $4b_1$ of SO_2F_2. The large polarities in the π systems of SO_2F_2 and $(NPF_2)_{3,4}$ follow the overall high polarities of the molecules as indicated by the atomic charges: $(P^{+1.51}N^{-0.36}F^{-0.57}{}_2)_3$ and $(P^{+1.56}N^{-0.49}F^{-0.53}{}_2)_4$ for the phosphazenes, $(S^{+1.96}O^{-0.43}{}_2F^{-0.55}{}_2)$ for sulfuryl fluoride. Another significant feature of the higher valence levels in SO_2F_2 and $(NPF_2)_{3,4}$ is the location of the nonbonding F(2p) band. With the assignments in this paper for SO_2F_2 and with the previous assignments for the phosphazenes,[9] the contributing experimental (vertical) ionization energies are 15.4, 16.6, and 17.2 eV in $(NPF_2)_3$, 15.9, 16.7, and 17.4 eV in $(NPF_2)_4$, and 16.68 and 18.31 eV in SO_2F_2. These bands, therefore, appear to progressively increase in energy, as a direct result of the inductive effect of the increasing P–N and S–O polarities through this series of molecules. Total electronic charge distributions are shown in Figure 7 for the SO and PN bonds of SO_2F_2 and $(NPF_2)_3$; the distribution in the SO plane of SO_2 is qualitatively similar to that for SO_2F_2.

Concluding Remarks

The $X\alpha$ SW calculations reported here give a good account of the vertical ionization energies of SO_2 and SO_2F_2. Some important similarities are found between the molecular orbital level structures of SO_2 and SO_2F_2 and between SO_2F_2 and $(NPF_2)_{3,4}$. In particular, the π states of heteromorphic symmetry in SO_2F_2, namely, $4b_2$ and $2a_2$, are found to be less stable than those of homomorphic symmetry, $4b_1$ and $6a_1$; this is consistent with our previous finding that the corresponding heteromorphic levels are absent in the ground states of $(NPF_2)_{3,4}$.[9] These calculations establish the presence of substantial π bonding in SO_2, SO_2F_2, and $(NPF_2)_{3,4}$, as well as significant participation by 3d orbitals at phosphorus and sulfur in both the σ and π bonds. The total 3d populations are 0.40 and 0.53 on sulfur in SO_2 and SO_2F_2, respectively, and 0.61 and 0.60 on phosphorus in $(NPF_2)_3$ and $(NPF_2)_4$;[9] for each molecule about one-third of the total 3d population is involved in the σ bonds. This work brings out, therefore, that neither the localized perfect pairing model nor the ionic resonance description provides an adequate model of chemical bonding in these molecules. We view this paper, and other related ones,[9,12] as contributing to the development of improved understandings of the electronic structures of molecules containing phosphorus or sulfur.

Acknowledgment. We are grateful for support of this work by the National Research Council of Canada. We also thank Professor N. L. Paddock and Dr. N. P. C. Westwood for many helpful discussions.

Registry No. SO_2, 7446-09-5; SO_2F_2, 2699-79-8.

References and Notes

(1) C. A. Coulson, *Nature (London)*, **221**, 1106 (1969).
(2) K. A. R. Mitchell, *Chem. Rev.*, **69**, 157 (1969).
(3) H. F. Schaefer, "The Electronic Structure of Atoms and Molecules", Addison-Wesley, Reading, Mass., 1972.
(4) J. C. Slater, "The Self Consistent Field for Molecules and Solids", McGraw-Hill, New York, N.Y., 1974.
(5) D. W. J. Cruickshank, *J. Chem. Soc.*, 5486 (1961).
(6) For example, B. H. Mahan, "University Chemistry", Addison-Wesley, Reading, Mass., 1975.
(7) *Chem. Soc., Spec. Publ.*, **No. 11** (1958).
(8) D. P. Craig and N. L. Paddock, "Nonbenzenoid Aromatics", Vol. 2, J. P. Synder, Ed., Academic Press, New York, N.Y., 1971.
(9) K. A. R. Mitchell, L. Noodleman, and N. L. Paddock, *Chem. Phys. Lett.*, **47**, 265 (1977).
(10) R. L. DeKock, D. R. Lloyd, I. H. Hillier, and V. R. Saunders, *Proc. R. Soc. London, Ser. A*, **328**, 401 (1972).
(11) D. Chadwick, D. C. Frost, F. G. Herring, A. Katrib, C. A. McDowell, and R. A. N. McLean, *Can. J. Chem.*, **51**, 1893 (1973).
(12) J. D. Head, K. A. R. Mitchell, L. Noodleman, and N. L. Paddock, *Can. J. Chem.*, **55**, 669 (1977).
(13) J. G. Norman, *Mol. Phys.*, **31**, 1191 (1976).
(14) K. Schwarz, *Phys. Rev. B*, **5**, 2466 (1972).
(15) J. C. Slater, *Adv. Quantum Chem.*, **6**, 1 (1972).
(16) K. H. Johnson, *Adv. Quantum Chem.*, **7**, 143 (1973).
(17) D. Kivelson, *J. Chem. Phys.*, **22**, 904 (1954).

(18) D. R. Lide, D. E. Mann, and R. M. Fristrom, *J. Chem. Phys.*, **26**, 736 (1957).
(19) S. Rothenberg and H. F. Schaefer, *J. Chem. Phys.*, **53**, 3014 (1970).
(20) L. S. Cederbaum, W. Domcke, W. von Niessen, and W. P. Kraemer, *Mol. Phys.*, **34**, 381 (1977).
(21) D. W. Turner, C. Baker, A. D. Baker, and C. R. Brundle, "Molecular Photoelectron Spectroscopy", Wiley-Interscience, London, 1970.
(22) The Xα SW calculations are, however, much less demanding on computer time. The full Xα SW calculation (in double precision) for SO_2, including the initial energy level determination, required 130 s on an IBM 370/168 computer. The near-Hartree–Fock calculations required about 7 h on a Univac 1108, a machine that is about 7 times slower. For SO_2, the Xα SW calculations are made in about one-thirtieth of the equivalent time required for the near-Hartree–Fock calculations, but for larger molecules the absolute savings in computation times are much greater with the Xα SW method.
(23) I. H. Hillier and V. R. Saunders, *Trans. Faraday Soc.*, **66**, 1544 (1970).
(24) The Mulliken charge distributions for the various restricted-basis-set calculations for SO_2 vary widely. This reflects both the real differences in the calculations and also the arbitrary aspects of the population analyses. From ref 19 and 23 representative atomic charges on S are +0.82 minimal s,p basis, +0.14 minimal s,p,d basis, +1.35 extended s,p basis, and +1.13 extended s,p,d basis. The calculated dipole moments according to these calculations are 1.24, 0.81, 2.83, and 2.28 D, respectively, and these values are to be compared with the experimental value of 1.63 D.
(25) D. R. Lide, D. E. Mann, and J. J. Comeford, *Spectrochim. Acta*, **21**, 497 (1965).
(26) M. W. Dougill, *J. Chem. Soc.*, 3211 (1963).

Contribution from the Chemistry Department, University of Texas, Austin, Texas 78712

Instabilities in the Elpasoite Structure: Structural-Phase Transformations and the Temperature-Dependent Raman Spectra of $Cs_2LiCo(CN)_6$ and $Cs_2LiIr(CN)_6$

B. I. SWANSON* and B. C. LUCAS

Received March 1, 1978

The structural-phase transformations in $Cs_2LiCo(CN)_6$ and $Cs_2LiIr(CN)_6$ have been probed using Raman scattering and optical microscopy. The goal of the present work has been to describe the structural distortions in terms of the allowed modes of vibration in the high-temperature cubic phase. The Ir^{3+} salt undergoes two phase transformations (T_c^1 = 418 K, T_c^2 = 335 K) while the Co^{3+} salt is observed optically to have one phase change (T_c^1 = 183 K). The 418 K phase change in the Ir^{3+} salt is first order involving rotation of the $Ir(CN)_6^{3-}$ octahedra. The 335 K transition is second order with the structural distortion proceeding along a soft Cs^+ translational mode. The phase transformation in $Cs_2LiCo(CN)_6$ involves a simultaneous distortion along the same two phonons. The structural instabilities for these two salts are the same as those observed earlier for other $R_2MM'L_6$ salts indicating that materials with the elpasoite structure may share a common lattice instability. The transition temperatures for $Cs_2LiM(CN)_6$ (M = $Cr^{3+} \rightarrow Co^{3+}$) salts correlate with the size of the Cs^+ site, as is consistent with the earlier suggestion that the driving force for the instabilities in these materials results from Cs^+ atoms occupying too large a site in the cubic lattice. As the Cs^+ site size decreases, the high-temperature cubic cell is stabilized thereby lowering the critical temperatures for the phase transformations. The correlation of Cs^+ site size and the critical temperature is not maintained in comparison of the Cr^{3+} and Ir^{3+} salts. The unusual behavior of the Ir^{3+} material has been attributed to a cooperative interaction of the external phonon instabilities with the internal forces of the $Ir(CN)_6^{3-}$ complex ion.

Displacive-phase transformations in crystalline solids have gained prominence in recent years, largely as a result of the compelling simplicity of the dynamics of second-order transitions.[1-3] The structural distortion accompanying a second-order displacive-phase change, the parallel to a reaction path for a chemical transformation, proceeds along one phonon direction in the vicinity of the critical temperature.[1,2] Furthermore, the structural distortion is continuous with temperature, thereby allowing the "reaction path" to be followed experimentally. The dynamics of chemical transformations, in addition to being considerably more complex, cannot be directly probed by experiment.

While there have been numerous studies of the dynamics of structural-phase changes in simple systems, such as the perovskites,[3,4] less is known of the lattice instabilities in more complex materials. We have been interested in salts containing octahedrally coordinated ML_6^{n-} complex ions, where the nature of the complex ion may influence the lattice instability.[5-8] Our principal goal in these studies has been to describe the dynamics of the structural change in terms of the allowed crystalline modes of vibration. Several temperature-dependent NQR studies of R_2MX_6 salts possessing the antifluorite structure (K_2PtCl_6,[9] K_2PdCl_6,[9] K_2IrCl_6,[9] K_2ReCl_6,[10-14] $(NH_4)_2PtBr_6$,[15] K_2PtBr_6,[17] K_2OsCl_6,[17] and K_2SnCl_6[18,19]) have been reported. These materials are observed to undergo multiple phase changes as temperature is lowered, and the NQR studies clearly indicate that the first transition in each involves rotation of the MX_6^{2-} octahedra. The lower temperature transformations are not well understood. However, we recently reported the temperature-dependent Raman scattering for K_2SnBr_6 in which a soft translational mode was implicated in the second phase change at 368 ± 5 K.[8] The first phase change in K_2SnBr_6 (T_c^1 = 399 K) involves rotation of the $SnBr_6^{2-}$ octahedra, as is consistent with the NQR studies of other antifluorite materials.[9-19]

The high-temperature phase of the antifluorite salts (cubic, *Fm3m*) is closely related to the elpasoite structure ($R_2MM'L_6$) adopted by many octahedrally coordinated trivalent metals. The antifluorite and elpasoite structures are identical except for the addition of the univalent M^+ cation in the 4b octahedral hole in the *Fm3m* cell of the latter. Salts with the elpasoite structure have been probed extensively in the past decade by workers interested in the structure and spectroscopy of ML_6^{3-} complex ions. The advantage of the $R_2MM'L_6$ salts in such studies is that the ML_6^{3-} ion occupies a site with O_h symmetry. Salts with three common cations, $M_3M'L_6$, generally have much lower symmetry. However, while high symmetry has made $R_2MM'L_6$ salts the preferred materials for studies of complexes of trivalent metals, few workers have worried about structural-phase transformations which may occur for elpasoites at reduced temperatures, despite the fact that many spectroscopic studies are carried out at low temperatures.

0020-1669/78/1317-2717$01.00/0